Received: 10 May 2022 | Revised: 2 June 2022 | Accepted: 6 June 2022

DOI: 10.1111/cas.15466

Cancer Science WILEY

ORIGINAL ARTICLE

Intercellular adhesion molecule-1-targeted near-infrared photoimmunotherapy of triple-negative breast cancer

Hiroshi Fukushima[1] | Takuya Kato[1] | Aki Furusawa[1] | Ryuhei Okada[1] | Hiroaki Wakiyama[1] | Hideyuki Furumoto[1] | Shuhei Okuyama[1] | Eisaku Kondo[2,3] | Peter L. Choyke[1] | Hisataka Kobayashi[1]

[1]Molecular Imaging Branch, Center for Cancer Research, NCI, NIH, Bethesda, Maryland, USA

[2]Division of Molecular and Cellular Pathology, Niigata University Graduate School of Medical and Dental Sciences, Niigata, Japan

[3]Division of Tumor Pathology, Near InfraRed PhotoImmunoTherapy Research Institute, Kansai Medical University, Hirakata, Japan

Correspondence
Hisataka Kobayashi, Molecular Imaging Branch, Center for Cancer Research, NCI, NIH, Bldg.10, Rm. B3B69, 10 Center Drive, Bethesda, MD 20892, USA.
Email: kobayash@mail.nih.gov

Funding information
Intramural Research Program of the NIH, NCI, Center for Cancer Research, Grant/Award Number: ZIA BC011513.

Abstract

Triple-negative breast cancer (TNBC) is the most aggressive subtype of breast cancer, and conventional chemotherapy and molecular-targeted therapies show limited efficacy. Near-infrared photoimmunotherapy (NIR-PIT) is a new anticancer treatment that selectively damages the cell membrane of cancer cells based on NIR light-induced photochemical reactions of the antibody (Ab)-photoabsorber (IRDye700Dx) conjugate and the cell membrane. TNBC is known to express several adhesion molecules on the cell surface providing a potential new target for therapy. Here, we investigated the therapeutic efficacy of intercellular adhesion molecule-1 (ICAM-1)-targeted NIR-PIT using xenograft mouse models subcutaneously inoculated with two human ICAM-1-expressing TNBC cell lines, MDAMB468-luc and MDAMB231 cells. In vitro ICAM-1-targeted NIR-PIT damaged both cell types in a NIR light dose-dependent manner. In vivo ICAM-1-targeted NIR-PIT in both models showed early histological signs of cancer cell damage, such as cytoplasmic vacuolation. Even among the cancer cells that appeared to be morphologically intact within 2 h post treatment, abnormal distribution of the actin cytoskeleton and a significant decrease in Ki-67 positivity were observed, indicating widespread cellular injury reflected in cytoplasmic degeneration. Such damage to cancer cells by NIR-PIT significantly inhibited subsequent tumor growth and improved survival. This study suggests that ICAM-1-targeted NIR-PIT could have potential clinical application in the treatment of TNBC.

KEYWORDS
cancer, cytoplasmic degeneration, ICAM-1, near-infrared photoimmunotherapy, triple-negative breast cancer

Abbreviations: Ab, antibody; APC, Ab-photoabsorber conjugate; BLI, bioluminescence imaging; DIC, differential interference contrast; DIG, digoxigenin; EGFR, epidermal growth factor receptor; FFPE, formalin-fixed paraffin-embedded; HER2, human epidermal growth factor receptor-2; ICAM-1, intercellular adhesion molecule-1; IR700, IRDye700DX; NIR-PIT, near-infrared photoimmunotherapy; pCK, pan-cytokeratin; PI, propidium iodide; ROI, region of interest; TBR, target-to-background ratio; TNBC, triple-negative breast cancer.

1 | INTRODUCTION

Breast cancer is the most common cancer worldwide in women, with 2,261,419 new cases and 684,996 deaths in 2020.[1] TNBC accounts for an estimated 15% of all breast cancers and is characterized by the lack of expression of estrogen and progesterone receptors and the lack of HER2 overexpression.[2] TNBC is more clinically aggressive compared with other subtypes of breast cancer. Patients with TNBC have poorer prognoses, with a 4-year overall survival rate of 77%, compared with 83–93% for other subtypes.[3] Chemotherapy is the mainstay treatment against TNBC, but response rates are low.[3] Although several molecular therapies targeting EGFR and c-KIT have been developed, they have failed to show significant benefit in clinical trials.[4,5] Therefore, there is an unmet need for a new form of molecular targeted therapy to treat TNBC.

NIR-PIT is a new anticancer therapeutic approach based on NIR light-induced activation of APCs.[6,7] The photoabsorber IR700, a silica-phthalocyanine dye, is conjugated to monoclonal Abs directed to target antigens on the surface of cancer cells.[7] After intravenous infusion of APCs, there is binding to cancer cells and exposure of the tumor to NIR light irradiation provokes axial ligand dissociation of IR700, converting it from being highly hydrophilic to being highly hydrophobic.[8] This reaction causes aggregation of APCs and APC-bound cell surface antigens, leading to significant damage to the cell membrane.[8] Immediately after NIR light irradiation, cancer cells start to swell, bleb, and rupture,[9] resulting in selective cancer cell killing with minimal damage to surrounding normal tissues. The benefit of utilizing NIR light is that it is harmless to cells by itself, and it penetrates deeper into tissues compared to other visible light. Preclinical studies have shown high therapeutic efficacy of NIR-PIT targeting various transmembrane proteins overexpressed in cancer cells, including EGFR,[10–12] HER2,[13,14] and prostate-specific membrane antigen.[15] Thus, with a suitable cell surface target and its cognate Ab, NIR-PIT can potentially become a powerful tool for treating TNBC.

ICAM-1 is a transmembrane protein and a cell adhesion molecule of the Ig superfamily. ICAM-1 is expressed at low levels in normal tissues, including the breast.[16] Under inflammatory conditions, leukocytes, endothelial cells, and T cells increase ICAM-1 expression, and ICAM-1 expression in these cells is associated with cell adhesion, leukocyte trafficking and migration, endothelial barrier function, and immune cell effector function.[17] ICAM-1 is overexpressed in various cancers such as lung cancer and pancreatic cancer.[18,19] Higher ICAM-1 expression was observed in TNBC compared with other subtypes of breast cancer.[20,21] In several recent studies, ICAM-1-targeted therapeutics have shown favorable results against TNBC.[20–22] Thus, we hypothesized that ICAM-1 is a potential target for NIR-PIT in the treatment of TNBC. In this study, we investigated the therapeutic efficacy of ICAM-1-targeted NIR-PIT using preclinical models of TNBC.

2 | MATERIALS AND METHODS

2.1 | Synthesis of IR700-conjugated anti-ICAM-1 Ab

One milligram of anti-human ICAM-1 Ab (6.7 nmol; clone R6-5-D6; Bio X Cell) was incubated with five-fold molar excess of IR700 NHS ester (10 mM in DMSO; LI-COR Biosciences) in 100 mM Na_2HPO_4 solution (pH 8.5) for 1 h at room temperature. The mixture was purified with PD-10 columns containing Sephadex G25 resin (GE Healthcare). The resulting APC was abbreviated as ICAM-1-IR700. ICAM-1-IR700 was analyzed by SDS-PAGE with a 4–20% gradient polyacrylamide gel (Life Technologies). Unconjugated Ab was used as a control. After electrophoresis at 80 V for 2.5 h, the gel was imaged with a Pearl Imager (LI-COR Biosciences) using the 700-nm fluorescence channel. The gel was then colored with colloidal blue staining to compare the molecular weight between the APC and nonconjugated Ab.

2.2 | Cell culture

Human TNBC cell lines MDAMB468 and MDAMB231 cells were obtained from the Division of Cancer Treatment and Diagnosis Tumor Repository, NCI Frederick. MDAMB468-luc cells were generated through stable transduction with RediFect Red-Fluc lentivirus from PerkinElmer. Cells were grown in culture flasks containing RPMI-1640 (Thermo Fisher Scientific) supplemented with 10% FBS and 100 IU/ml penicillin/streptomycin (Thermo Fisher Scientific) in a humidified incubator at 37°C under an atmosphere of 95% air and 5% CO_2 for no more than 30 passages.

2.3 | In vitro ICAM-1 expression analysis

To assess in vitro ICAM-1 expression on MDAMB468-luc or MDAMB231 cells, 2×10^5 cells were collected in 100 μL PBS and incubated with PE-labeled anti-human ICAM-1 Ab (clone HA58; BioLegend) or its PE-labeled mouse IgG1κ isotype control (clone MOPC-21; BioLegend) as well as Fixable Viability Dye (Thermo Fisher Scientific) for 30 min at 4°C. After washing with PBS, the fluorescence of the cells was analyzed by BD FACSLyric (BD Biosciences) and FlowJo software (BD Biosciences).

2.4 | In vitro cell-specific binding analysis

To verify the in vitro binding of ICAM-1-IR700 to MDAMB468-luc or MDAMB231 cells, 2×10^5 cells were collected in 100 μL of PBS and incubated with 1 μg of ICAM-1-IR700 for 30 min at 4°C. After washing with PBS, the fluorescence of the cells was analyzed by BD FACSLyric and FlowJo software. To validate the specific binding of

ICAM-1-IR700, 10-fold molar excess of unconjugated anti-ICAM-1 Ab (clone R6-5-D6; Bio X Cell) was added 30 min before the incubation with ICAM-1-IR700. Dead cells were excluded from the analysis based on the staining with Fixable Viability Dye.

2.5 | In vitro fluorescence microscopy

MDAMB468-luc or MDAMB231 cells were seeded at 2×10^4 on glass-bottomed dishes and incubated for 24 h. Cells were incubated with 100 μl fresh culture medium containing 1 μg ICAM-1-IR700 for 1 h at 37°C. The cells were washed with PBS and observed with a fluorescence microscope (IX81; Olympus America). Transmitted light DIC images were obtained, and IR700 was detected using the filter set, which included a 608–668 nm excitation filter and a 672–712 nm bandpass emission filter. The cells were then exposed to NIR light irradiation (690 nm, 150 mW/cm^2, 50 J/cm^2) using an ML7710 laser system (Modulight). The DIC images were acquired again 30 min after NIR light irradiation.

2.6 | In vitro NIR-PIT

MDAMB468-luc or MDAMB231 cells were seeded onto 24-well plates at 1×10^5 per well in quadruplicate in 1 mL medium and incubated for 24 h. Cells were incubated with 200 μl fresh culture medium containing 2 μg ICAM-1-IR700 for 1 h at 37°C. After washing with PBS, phenol-red-free medium was added. NIR laser-light (690 nm, 150 mW/cm^2) using an ML7710 laser system was applied. One hour after NIR-PIT, the cytotoxic effects of NIR-PIT with ICAM-1-IR700 were determined by two types of cell viability assay. For PI flow cytometric assay, cells were harvested and stained with 1 μg/mL PI (Life Technologies). The percentage of PI-stained cells was determined by BD FACSLyric flow cytometry and FlowJo software. Cell proliferation was evaluated using an MTT assay kit (Sigma Aldrich) as described previously.[23] For relative quantification, the value of absorbance in each group was normalized to the untreated control.

2.7 | Animal models

Female homozygote athymic nude mice, 6–8 weeks old, were purchased from Charles River Laboratories. MDAMB468-luc (4×10^6) or MDAMB231 (1×10^6) cells were inoculated into the right dorsum of mice. Tumor volumes were evaluated three times per week by a caliper and calculated as follows: tumor volume (mm^3) = length × width^2 × 0.5. The mice were killed with CO_2 when the tumor volume reached 2000 mm^3.

2.8 | In vivo fluorescence imaging

Tumor-bearing mice were injected with ICAM-1-IR700 (100 μg) into the lateral tail vein. Serial dorsal fluorescence images were obtained with the 700 nm fluorescence channel of a Pearl Imager (LI-COR Bioscience). The images were analyzed with Pearl Cam Software (LI-COR Bioscience). Regions of interest were drawn on the tumor and the nontumoral region of the contralateral side. TBR was calculated as (mean fluorescence intensity of the tumor)/(mean fluorescence intensity of the nontumoral region of the contralateral side).

2.9 | In vivo NIR-PIT

Tumor-bearing mice were randomized into three groups as follows: (i) no treatment (Control), (ii) intravenous injection of ICAM-1-IR700 only (APC-IV), and (iii) intravenous injection of ICAM-1-IR700 followed by NIR-PIT (NIR-PIT). ICAM-1-IR700 (100 μg) was injected 9 and 25 days after MDAMB468-luc and MDAMB231 cell inoculation, respectively (day −1). The NIR laser-light (690 nm, 150 mW/cm^2, 50 J/cm^2) was administered to the tumor 24 h (day 0) and 48 h (day 1) after ICAM-1-IR700 injection. Upon NIR light irradiation, a piece of aluminum foil with a hole of approximately 1 cm diameter was placed over the mouse; then NIR light was irradiated to the tumor through the hole to ensure that the NIR light irradiation was limited to the tumor site. Serial fluorescence images and white light images were obtained using a Pearl Imager with the 700 nm fluorescence channel. Acute treatment efficacy was evaluated with BLI analysis, in which D-luciferin (15 mg/mL, 200 μL; Gold Biotechnology) was injected intraperitoneally, and luciferase activity was analyzed with a Photon Imager and M3 Vision Software (Biospace Lab). The ROIs were drawn to include the entire tumor.

2.10 | Histological analysis

Tumor-bearing mice were randomized into the Control, APC-IV, and NIR-PIT groups. For the NIR-PIT group, mice were exposed to NIR light (690 nm, 150 mW/cm^2, 50 J/cm^2) 24 h after ICAM-1-IR700 injection. To evaluate histological changes after NIR-PIT, tumors were harvested 2 h after NIR light irradiation. The FFPE sections were prepared and stained with hematoxylin and eosin (H&E).

2.11 | Detection of DIG-labeled Ab by multiplex immunohistochemistry

Anti-ICAM-1 Ab (clone R6-5-D6; Bio X Cell) or its mouse IgG2a isotype control (clone C1.18.4; Bio X Cell) (1 mg) was labeled with DIG by incubating 1 mg Ab and 50 μg DIG-NHS-ester (Thermo Fisher Scientific) using a similar method to IR700 conjugation. The resulting DIG-labeled Abs were abbreviated as ICAM-1-DIG and isotype-DIG, respectively. Tumor-bearing mice were injected with ICAM-1-DIG or isotype-DIG (100 μg) into the lateral tail vein. Tumors were harvested 24 h after injecting DIG-labeled Abs. The distribution of DIG-labeled Abs was analyzed in FFPE sections by multiplex immunohistochemistry using anti-DIG Ab (clone 9H27L19; Thermo Fisher Scientific).

2.12 | Immunohistochemistry

Multiplex immunohistochemistry was carried out as described previously,[24,25] using an Opal Automation IHC Kit (Akoya Bioscience) and Bond RXm autostainer (Leica Biosystems). The sections were stained with DAPI and the following Abs: anti-β-actin (rabbit poly; Abcam; 1:500), anti-CD45 (clone D3F8Q; Cell Signaling Technology; 1:500), anti-DIG (clone 9H27L19; Thermo Fisher Scientific; 1:500), anti-Ki-67 (clone D3B5; Cell Signaling Technology; 1:500), and anti-pCK (rabbit poly; Bioss Antibodies; 1:250). Stained slides were mounted with ProLong Diamond (Thermo Fisher Scientific) and imaged with a Mantra Quantitative Pathology Workstation (Akoya Biosystems). The obtained images were analyzed with inForm Tissue Finder software (Akoya Biosystems). To calculate the percentage of Ki-67 positive cancer cells, inForm software was trained to detect tissue and cell phenotypes using machine-learning algorithms based on the following criteria: areas with pCK expression = tumor, other areas = stroma, $pCK^{+}CD45^{-}$ cells = cancer cells, $pCK^{-}CD45^{+}$ = blood cells, and $pCK^{-}CD45^{-}$ = other cells. inForm software computed the percentage of Ki-67 positive cells among cancer cells. The average percentage was calculated from five images for each specimen. Single-marker immunohistochemistry was undertaken as described previously.[26] Slides were incubated with anti-E-cadherin Ab (clone 36/E-Cadherin; BD Biosciences; 1:500) and subsequently with N-Histofine Simple Stain MAX PO (MULTI) (Nichirei Biosciences).

2.13 | Statistical analysis

Data are expressed as means ± SEM. Statistical analyses were undertaken with GraphPad Prism (GraphPad Software). A one-way ANOVA followed by Tukey's test was used to compare multiple groups. For luciferase activity and tumor volumes, a repeated measures two-way ANOVA followed by Tukey's test was used. The cumulative probability of survival based on tumor volume (2000 mm^3) was estimated with a Kaplan–Meier method, and the results were compared by the log–rank test with Bonferroni correction. $p < 0.05$ was considered significant.

3 | RESULTS

3.1 | Conjugation of IR700 to anti-ICAM-1 Ab

IR700 was conjugated to anti-ICAM-1 Ab and the synthesized APC (ICAM-1-IR700) was analyzed by SDS-PAGE. ICAM-1-IR700 was of the same molecular weight as unconjugated anti-ICAM-1 Ab but a fluorescence of 700 nm was detected only in ICAM-1-IR700 (Figure 1A).

3.2 | Expression of ICAM-1 in TNBC cell lines

Expression of ICAM-1 on the surface of MDAMB468-luc and MDAMB231 cells was evaluated in vitro. ICAM-1 was highly expressed in MDAMB468-luc cells, whereas its expression was modest in MDAMB231 cells (Figure 1B). Next, to assess the binding of ICAM-1-IR700 to MDAMB468-luc and MDAMB231 cells in vitro, they were incubated with ICAM-1-IR700 and analyzed by flow cytometry. MDAMB468-luc cells showed a high IR700 fluorescence signal (Figure 1C, top panel). The fluorescence signal of MDAMB231 cells was detected but was lower than that of MDAMB468-luc cells (Figure 1C, bottom panel). These signals were completely blocked by adding an excess of unconjugated anti-ICAM-1 Ab (Figure 1C), indicating that ICAM-1-IR700 specifically binds to ICAM-1 expressed on the surface of MDAMB468-luc and MDAMB231 cells.

3.3 | Target cell killing efficacy of in vitro ICAM-1-targeted NIR-PIT

We evaluated the cell killing efficacy of in vitro ICAM-1-targeted NIR-PIT using MDAMB468-luc and MDAMB231 cells. The cells were incubated with ICAM-1-IR700, and cell morphology was microscopically examined after NIR light irradiation. In MDAMB468-luc cells, IR700 fluorescence was detected before NIR light irradiation, and cellular swelling was observed immediately after NIR light irradiation (Figure 1D, top panels). Although IR700 fluorescence was dimmer in MDAMB231 cells, NIR light irradiation caused bleb formation of cells (Figure 1D, bottom panels). Cell membrane damage after in vitro ICAM-1-targeted NIR-PIT was quantitatively evaluated using PI flow cytometric assay. The percentage of PI-positive cells increased after NIR-PIT in MDAMB468-luc cells in a light dose-dependent manner (Figure 1E). Treatment with ICAM-1-IR700 alone or NIR light irradiation alone did not affect cell viability. Analogous results were obtained in MDAMB231 cells, but there was less cell killing than in MDAMB468-luc cells (Figure 1F). Moreover, the MTT assay showed significantly lower metabolic activity after NIR-PIT compared with the control in MDAMB468-luc cells (Figure 1G), while there was no apparent reduction of metabolic activity after NIR-PIT in MDAMB231 cells (Figure 1H).

3.4 | Anti-ICAM-1 Ab delivery to cancer cells in vivo

To evaluate whether anti-ICAM-1 Ab is delivered to MDAMB468-luc and MDAMB231 cells in vivo, either ICAM-1-DIG or isotype-DIG was infused into tumor-bearing mice, then DIG distribution in the tumors was analyzed by multiplex immunohistochemistry. In MDAMB468-luc and MDAMB231 tumors, ICAM-1-DIG was detected on the cell surface of pCK-positive cancer cells (Figure 2). Isotype-DIG was slightly detected in both the tumors, which was likely to be mediated by Fc receptor binding. These results indicated that anti-ICAM-1 Ab was successfully delivered to the tumor tissue and bound to the surface of cancer cells in both MDAMB468-luc and MDAMB231 tumors.

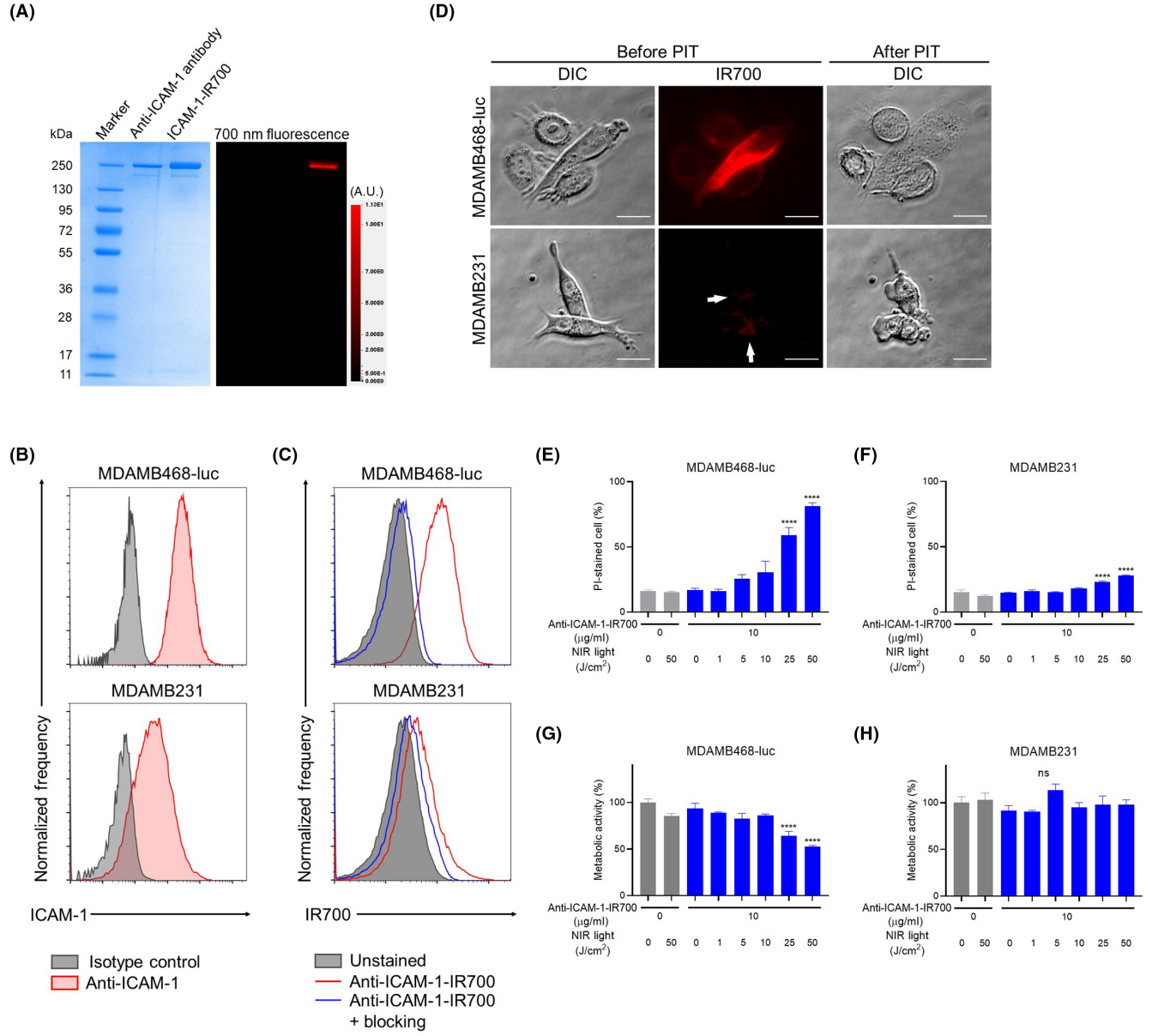

FIGURE 1 In vitro ICAM-1-targeted NIR-PIT in MDAMB468-luc and MDAMB231 cells. (A) Evaluation of ICAM-1-IR700 by SDS-PAGE (left, colloidal blue staining; right, 700 nm fluorescence). Unconjugated anti-ICAM-1 Ab was used as a control. Fluorescence intensity was confirmed in the band of ICAM-1-IR700. A.U., arbitrary units. (B) Flow cytometric analysis of in vitro ICAM-1 expression on MDAMB468-luc and MDAMB231 cells. (C) Detection of ICAM-1-IR700 bound to MDAMB468-luc and MDAMB231 cells by flow cytometric analysis. (D) Microscopic observation of cancer cells before and after in vitro ICAM-1-targeted NIR-PIT (images, ×400; scale bar, 20 μm). White arrows indicate IR700 fluorescence in MDAMB231 cells. DIC, differential interference contrast. (E,F) Membrane damage of MDAMB468-luc (E) and MDAMB231 (F) cells induced by in vitro ICAM-1-targeted NIR-PIT was measured with the dead cell count using PI staining ($n = 4$; one-way ANOVA followed by Tukey's test). ****$p < 0.0001$ vs. untreated control. (G, H) Metabolic activity of MDAMB468-luc (G) and MDAMB231 (H) cells after in vitro ICAM-1-targeted NIR-PIT was measured by MTT assay ($n = 4$; one-way ANOVA followed by Tukey's test). ****$p < 0.0001$. ns, not significant vs. untreated control

3.5 | In vivo fluorescence imaging studies of ICAM-1-IR700

Serial in vivo fluorescent imaging of ICAM-1-IR700 was undertaken after APC injection using MDAMB468-luc (Figure 3A) and MDAMB231 (Figure 3B) tumor-bearing mice. The fluorescence intensity of ICAM-1-IR700 at the tumor site was the highest 24 h after APC injection, and it gradually decreased thereafter in both models (Figure 3C). The TBR of ICAM-1-IR700 increased up to 24 h after treatment and was stable thereafter in both models during the period of observation (Figure 3D). Because of high fluorescence intensity at the tumor site and high TBR 24 h after APC injection, first NIR light irradiation was planned 24 h after APC injection to get the maximal difference between tumor and background normal tissue for in vivo NIR-PIT studies.

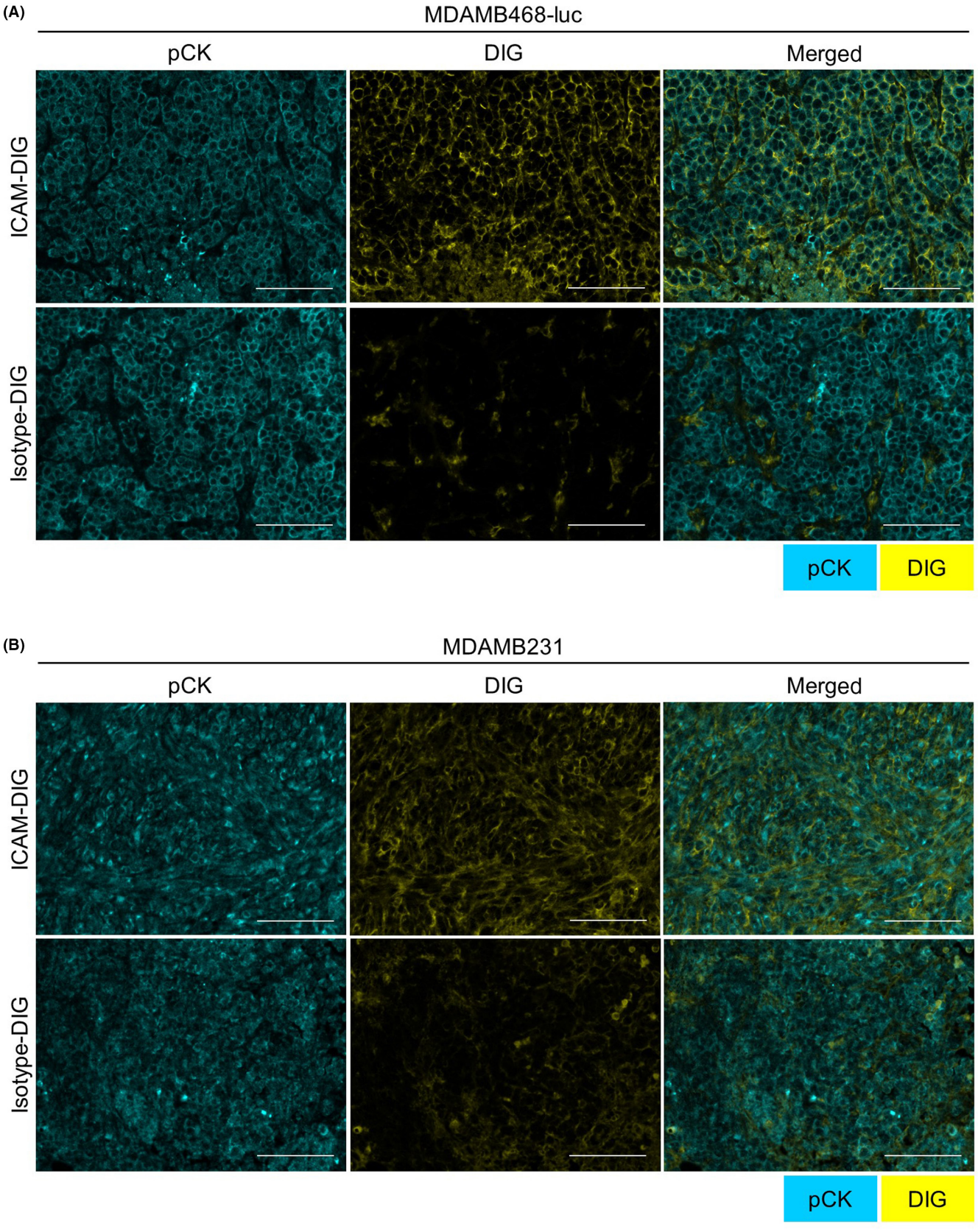

FIGURE 2 Delivery of ICAM-1 Ab to MDAMB468-luc and MDAMB231 cells in vivo. Tumors were harvested 24 h after injecting ICAM-1-DIG or isotype-DIG into mice and its distribution in MDAMB468-luc (A) and MDAMB231 (B) tumors was examined by multiplex immunohistochemistry (images, ×200; scale bar, 100 μm). Pan-cytokeratin (pCK) expression and DIG are shown in cyan and yellow, respectively.

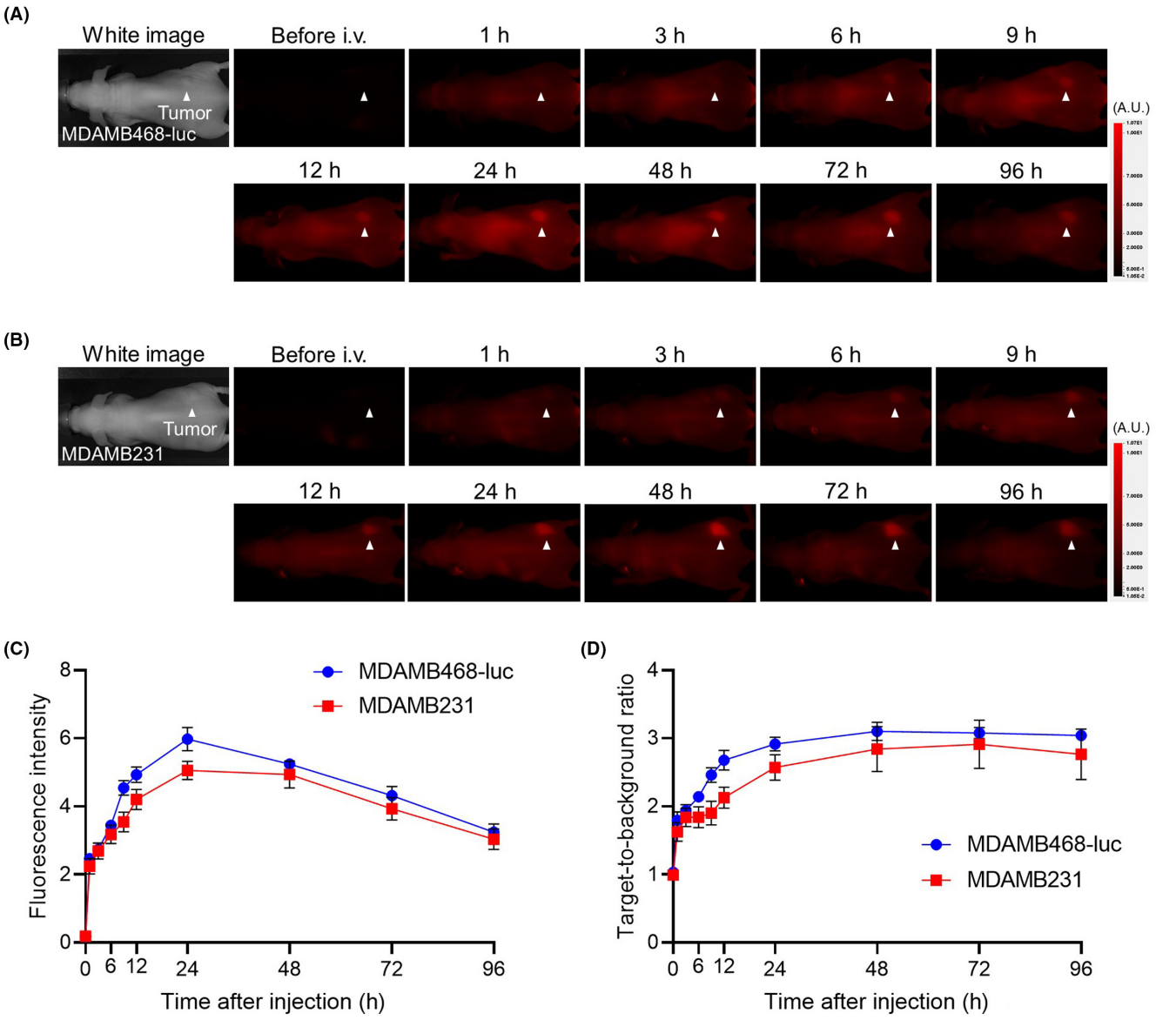

FIGURE 3 In vivo fluorescence imaging of ICAM-1-IR700. (A,B) Representative fluorescence images at 700 nm in a MDAMB468-luc (A) and MDAMB231 (B) tumor-bearing mouse. All images were acquired at the indicated time points after injecting ICAM-1-IR700 into mice. A.U., arbitrary units. (C) Quantitative analysis of 700 nm fluorescence intensity at the tumor site after injecting ICAM-1-IR700 ($n = 6$). (D) Quantitative analysis of target-to-background ratio after injecting ICAM-1-IR700 ($n = 6$)

3.6 | In vivo ICAM-1-targeted NIR-PIT inhibits the growth of MDAMB468-luc tumors

Therapeutic efficacy of in vivo ICAM-1-targeted NIR-PIT was evaluated in MDAMB468-luc tumor-bearing mice. Figure 4A shows the treatment and imaging schedule. All APC-injected mice clearly showed a 700 nm fluorescent signal at the tumor site just before NIR light irradiation. The first NIR light irradiation immediately reduced this signal, indicating photobleaching of the conjugated IR700. One day after the first NIR light irradiation, the fluorescence signal at the tumor site reaccumulated and immediately declined after the second NIR light irradiation (Figure 4B). Bioluminescence imaging was utilized to assess the cellular activity of cancer cells after the NIR-PIT in the early phase (Figure 4C). The luciferase activity in the NIR-PIT group decreased rapidly after the first NIR light irradiation. The decreased signal gradually recovered over time but still was significantly lower than that of the Control and APC-IV groups (Figure 4D). In the NIR-PIT group, the tumor size initially shrank after NIR light irradiation, then grew back over time, however, the growth was significantly slower than in the Control and APC-IV groups (Figure 4E). The NIR-PIT group had significantly improved survival compared with the Control and APC-IV groups (Figure 4F). There were no significant differences in BLI signal, tumor growth, or survival between the Control and APC-IV groups.

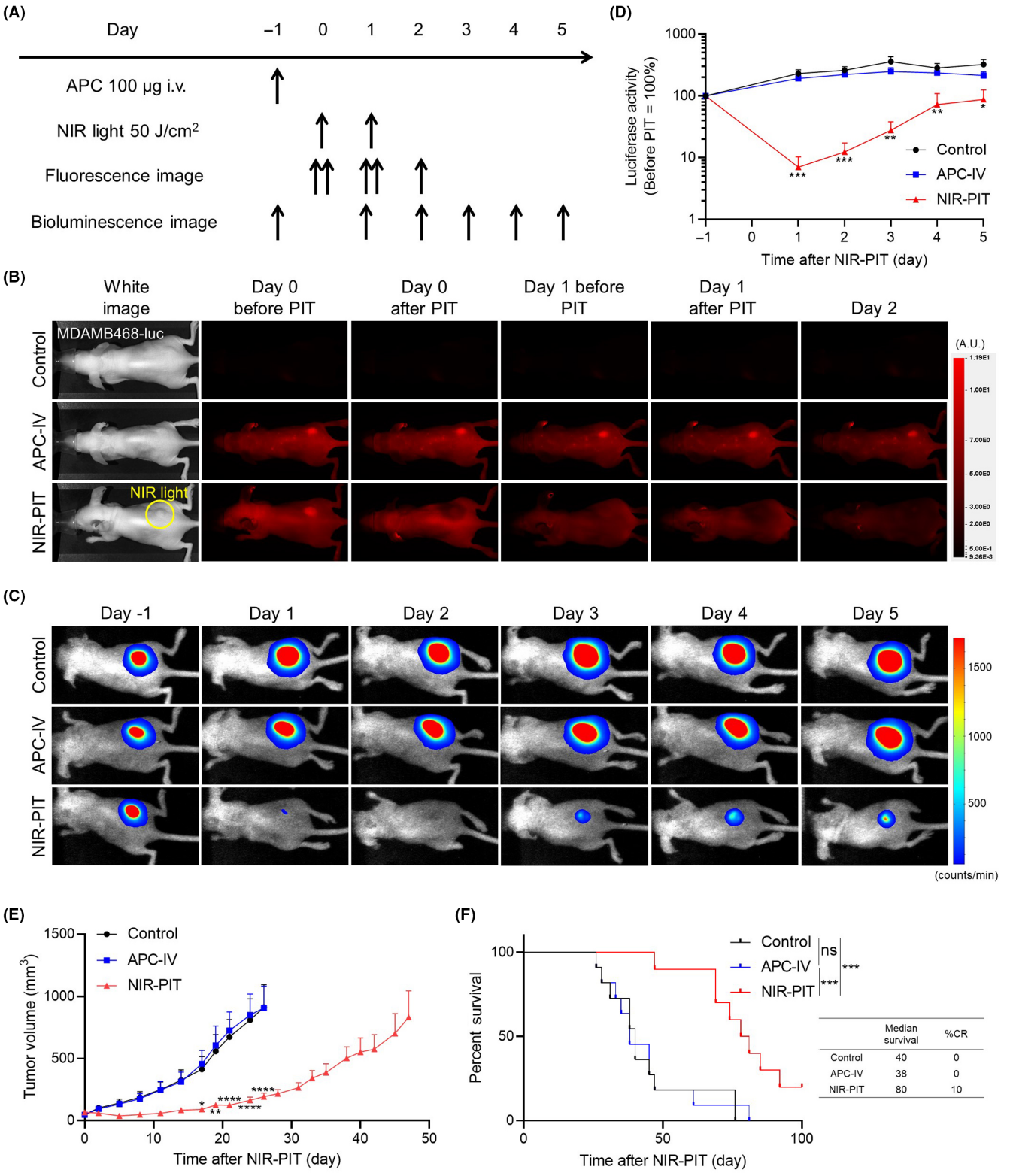

FIGURE 4 Efficacy of in vivo ICAM-1-targeted NIR-PIT against MDAMB468-luc tumors. (A) Treatment schedule. (B) Representative fluorescent imaging at 700 nm before and after NIR-PIT in MDAMB468-luc tumor-bearing mice. A.U., arbitrary units. (C) Representative bioluminescence imaging (BLI) before and after NIR-PIT in MDAMB468-luc tumor-bearing mice. (D) Luciferase activity measured by BLI ($n = 10–11$; mean ± SEM; repeated measures two-way ANOVA followed by Tukey's test). $^{*}p < 0.05$; $^{**}p < 0.01$; $^{***}p < 0.001$ vs. Control. (E) Tumor volume curves ($n = 10–11$; mean ± SEM; repeated measures two-way ANOVA followed by Tukey's test. $^{*}p < 0.05$; $^{**}p < 0.01$; $^{****}p < 0.0001$ vs. Control. (F) Survival curves ($n = 10–11$, log–rank test with Bonferroni correction). $^{***}p < 0.001$. %CR, % complete response; APC, Ab-photoabsorber conjugate; ns, not significant

3.7 | In vivo ICAM-1-targeted NIR-PIT inhibits growth of MDAMB231 tumors

Therapeutic efficacy of in vivo ICAM-1-targeted NIR-PIT was also evaluated in MDAMB231 tumor-bearing mice. The treatment and imaging schedule is shown in Figure 5A. The 700 nm fluorescence signal at the tumor site showed a similar trend to that of MDAMB468-luc tumors (Figure 5B); in the NIR-PIT group, the signal immediately decreased after the first and second NIR light irradiations. The ICAM-1-targeted NIR-PIT significantly inhibited tumor growth compared with the Control and APC-IV groups (Figure 5C), but its efficacy was less than that in MDAMB468-luc models. The NIR-PIT group showed significantly longer survival compared with the Control and APC-IV groups (Figure 5D). There were no significant differences in tumor growth or survival between the Control and APC-IV groups.

3.8 | Early histological changes after in vivo ICAM-1-targeted NIR-PIT

We examined the histology of the tumors 2 h after NIR-PIT to histologically evaluate direct cytotoxic effects of in vivo ICAM-1-targeted NIR-PIT. In H&E staining of MDAMB468 and MDAMB231 tumors, most cancer cells appeared to be morphologically intact after NIR-PIT. Yet, cytoplasmic vacuolation, which suggests cytoplasmic degeneration, was observed in a subset of cancer cells after NIR-PIT (Figure 6A). Interestingly, nuclear structures were maintained in these cells. Such histological changes were not seen in the Control group. Next, actin cytoskeleton distribution was assessed by multiplex immunohistochemistry to investigate whether NIR-PIT affects the cytoplasm of cancer cells despite appearing morphologically intact in H&E staining. Actin fibers were uniformly spread across the entire cytoplasm of cancer cells

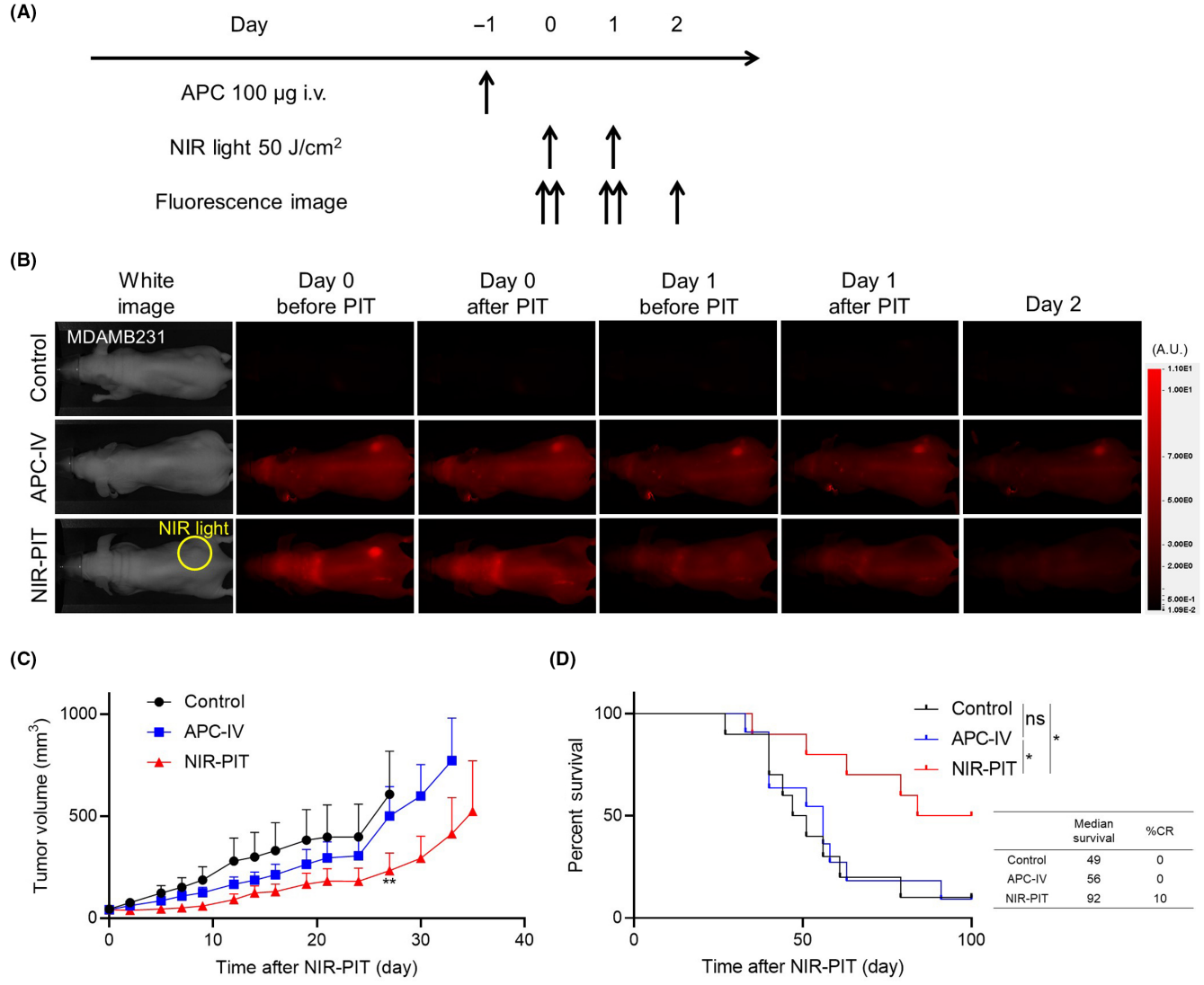

FIGURE 5 Efficacy of in vivo ICAM-1-targeted NIR-PIT against MDAMB231 tumors. (A) Treatment schedule. (B) Representative fluorescent imaging at 700 nm before and after NIR-PIT in MDAMB231 tumor-bearing mice. A.U., arbitrary units. (C) Tumor volume curves ($n = 10–11$; mean ± SEM; repeated measures two-way ANOVA followed by Tukey's test). $^{**}p < 0.01$ vs. Control. (D) Survival curves ($n = 10–11$, log–rank test with Bonferroni correction). $^{*}p < 0.05$. %CR, % complete response; APC, Ab-photoabsorber conjugate; ns, not significant

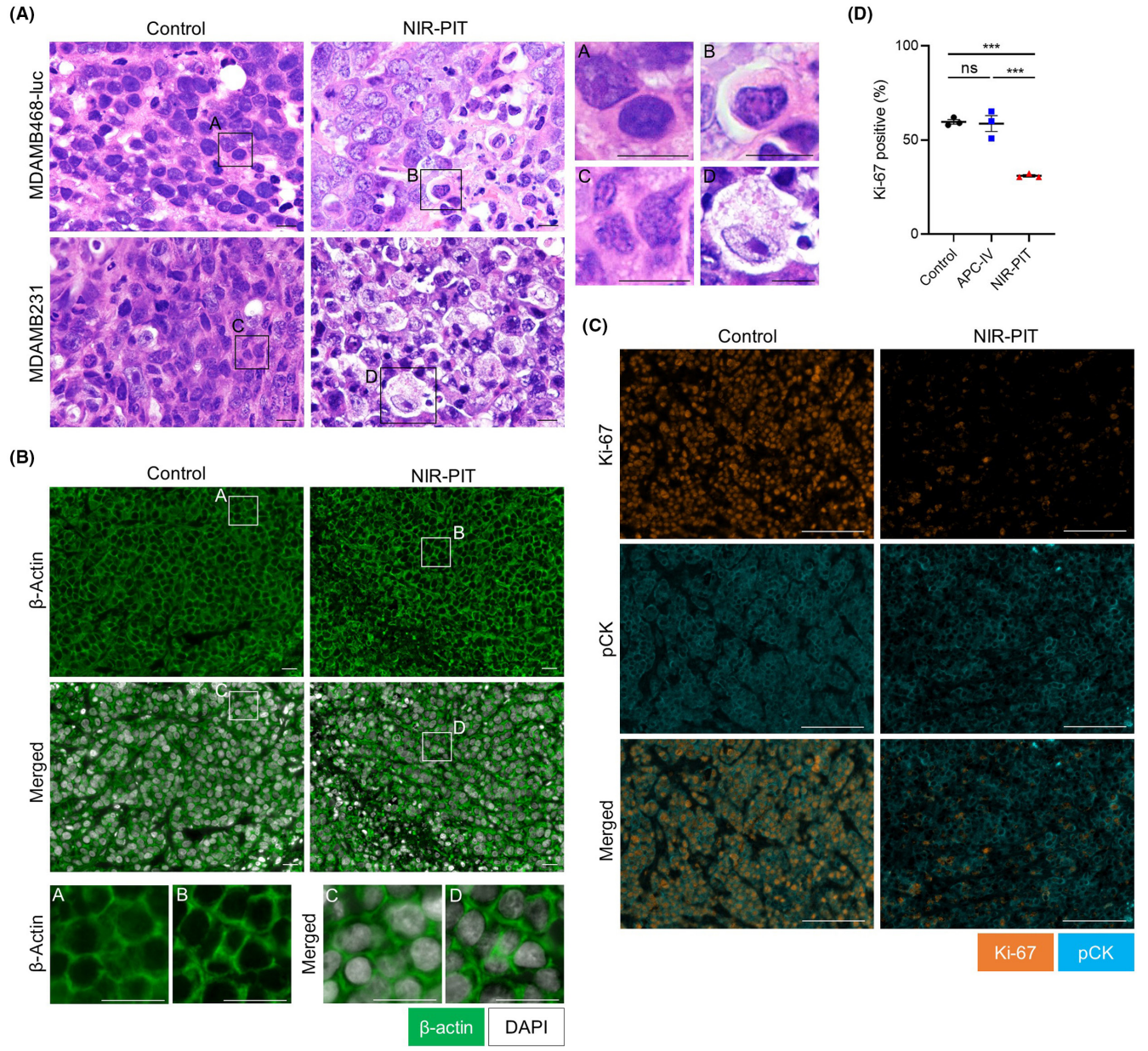

FIGURE 6 Early histological changes after in vivo ICAM-1-targeted NIR-PIT. Tumor tissue histology was examined 2 h after NIR-PIT. (A) H&E staining of MDAMB468-luc and MDAMB231 tumors after NIR-PIT (images, ×1000; scale bar, 10 μm). Insets (A–D) are enlarged and displayed in the right panels. (B) Evaluation of actin cytoskeleton distribution among cancer cells in MDAMB468-luc tumors by multiplex immunohistochemistry (images, ×400; scale bar, 20 μm). Actin cytoskeleton is shown in green; DAPI counterstaining is shown in white. Insets (A–D) are enlarged and displayed in the bottom panels. (C,D) Evaluation of Ki-67 positivity among cancer cells in MDAMB468-luc tumors by multiplex immunohistochemistry. (C) Representative pictures of Ki-67 and pan-cytokeratin (pCK) expression (images, ×200; scale bar, 100 μm). Ki-67 and pCK expression is shown in orange and cyan, respectively. (D) Comparison of the percentage of Ki-67 positive cancer cells among the three groups ($n = 3$; one-way ANOVA followed by Tukey's test). ***$p < 0.001$. APC, Ab-photoabsorber conjugate; ns, not significant

in the Control group (Figures 6B and S1). In the NIR-PIT group, the actin cytoskeleton was abnormally distributed in most cancer cells (Figures 6B and S1). This finding prompted us to assess Ki-67 expression among cancer cells to evaluate whether NIR-PIT exerted significant damage. In MDAMB468-luc tumors, the percentage of Ki-67 positive cancer cells was significantly lower in the NIR-PIT group compared with the Control and APC-IV groups (Figure 6C,D). Ki-67 staining was not significantly decreased by NIR-PIT in MDAMB231 tumors (Figure S2). In MDAMB468-luc tumors, reduction of E-cadherin expression was also observed in the NIR-PIT group (Figure S3).

4 | DISCUSSION

In this study, ICAM-1-targeted NIR-PIT achieved high therapeutic efficacy in TNBC using ICAM-1-IR700 and NIR light. The ICAM-1-targeted NIR-PIT successfully inhibited tumor growth and improved

survival in TNBC xenograft models. Histological analysis revealed that in vivo ICAM-1-targeted NIR-PIT induced early histological changes such as cytoplasmic vacuolation. However, most cancer cells appeared to be morphologically intact on H&E staining. Immunohistochemical analyses showed an abnormal distribution of the actin cytoskeleton in treated cancer cells that appeared intact on H&E staining. These findings suggest that NIR-PIT caused extensive cytoplasmic degeneration, reflecting the cytotoxic mechanism of NIR-PIT, which is characterized by damage to the cell membrane.[8] Reduction of E-cadherin expression also suggests significant cell membrane damage following NIR-PIT. In addition, ICAM-1-targeted NIR-PIT significantly decreased Ki-67 staining, indicating widespread functional damage to cellular proliferation.

In this study, in vitro ICAM-1-targeted NIR-PIT elicited significant cytotoxicity in MDAMB468-luc cells, but its therapeutic efficacy was modest in MDAMB231 cells. This result is likely because the expression of ICAM-1 is lower in MDAMB231 cells than in MDAMB468-luc cells in vitro. Initial tumor shrinkage and tumor growth suppression by in vivo ICAM-1-targeted NIR-PIT were more evident in MDAMB468-luc tumor models, but both models indicated tumor suppression resulting in significantly extended survival. In this study, we used immunodeficient mice that lack adaptive immunity; however, NIR-PIT might stimulate innate immunity in immunodeficient mice. This could partly explain the observed efficacy of in vivo ICAM-1-targeted NIR-PIT against MDAMB231 tumors. Because of the potential of NIR-PIT to activate adaptive immune cells against cancer cells,[25,27,28] in vivo ICAM-1-targeted NIR-PIT could show higher efficacy in immunocompetent mouse models. We used immunodeficient mouse models in this study to test the direct cell killing efficacy against human TNBC models; however, the efficacy of ICAM-targeted NIR-PIT in immunocompetent mouse models should be investigated in future studies.

There are several examples of ICAM-1-targeted Ab agents that are intended to block ICAM-1 or to deplete ICAM-1-expressing cancer cells through Fc-dependent effector mechanisms such as Ab-dependent complement-mediated cytotoxicity or complement-dependent cytotoxicity.[29,30] However, intravenous infusion of ICAM-1-IR700 alone showed almost no therapeutic effect on tumor growth or survival of mice in this study. Therefore, at least at the dose used in this study, intravenous infusion of ICAM-1-IR700 alone is not effective enough to kill ICAM-1-expressing cancer cells.

ICAM-1 has various roles in the development and progression of cancer. ICAM-1 is implicated in cluster formation of circulating tumor cells and their homing to secondary organs. Additionally, ICAM-1 helps cancer cells transmigrate through the vascular endothelium.[17] Thus, ICAM-1 can contribute to enhanced invasiveness of cancer cells and the development of metastatic lesions. ICAM-1 was identified as a metastatic initiator by comparing single-cell sequencing profiles between primary and metastatic tumors in TNBC patient-derived xenografts.[31] Thus, ICAM-1-targeted NIR-PIT could selectively deplete cancer cells with high metastatic potential in heterogeneous cancer cell populations. Indeed, ICAM-1 overexpression was associated with higher rates of recurrence in patients with estrogen receptor-negative breast cancer.[32]

This study has several limitations. First, we used human cell line-derived xenografts in immunodeficient mice in this study. Thus, we could not evaluate the effect of ICAM-1-targeted NIR-PIT on immune cells. Expression of ICAM-1 can be observed in various normal cells such as leukocytes, endothelial cells, and T cells.[17] Pro-inflammatory stimulation can increase ICAM-1 expression in these cells.[17] The therapeutic effect of NIR-PIT depends not only on direct cancer cell killing but also on the activation of anticancer immunity.[25,27,28] Ideally, to obtain maximal therapeutic effects, immune cells in the tumor microenvironment should be intact after NIR-PIT. Thus, the effect of ICAM-1-targeted NIR-PIT on immune cells remains to be elucidated using immunocompetent mouse models. Second, ICAM-1-targeted NIR-PIT did not significantly decrease the percentage of Ki-67 positive cancer cells in MDAMB231 tumors, probably because the time course for significant cellular damage by NIR-PIT can vary by cell type and expression level of target molecules that could alter APC binding to cancer cells in the tumor. Third, we evaluated the therapeutic efficacy of ICAM-1-targeted NIR-PIT only in TNBC. ICAM-1 might be a target molecule for NIR-PIT against other cancers that express it. Previous studies showed that ICAM-1 expression was detected in 41%, 50%, and 44% of non-small-cell lung cancers,[33] gastric cancers,[34] and colorectal cancers.[35] Further research is necessary to evaluate the therapeutic efficacy of ICAM-1-targeted NIR-PIT in mouse models of these cancers. Finally, we did not compare therapeutic efficacy between ICAM-1-targeted NIR-PIT and EGFR-targeted NIR-PIT in TNBC. We previously reported high therapeutic efficacy of EGFR-targeted NIR-PIT in TNBC mouse models.[36] It should be elucidated that either therapy alone or combination therapy is more effective in TNBC mouse models.

In conclusion, we showed that ICAM-1-targeted NIR-PIT significantly suppressed tumor growth and prolonged survival using human TNBC xenograft mouse models. Therefore, ICAM-1-targeted NIR-PIT is a promising targeted therapy against TNBC and could be a good candidate for human trials.

AUTHOR CONTRIBUTIONS

All authors read and approved the final version of the manuscript. H.F. mainly designed and conducted experiments, performed analysis, verifying data and wrote the manuscript; T.K., A.F., R.O., H.W., H.F., S.O., and T.N. performed experiments and analysis; E.K. prepared the specimen and evaluated the pathological findings; P.L.C. wrote the manuscript and supervised the project; and H.K. planned and initiated the project, designed and conducted experiments, verifying data, wrote and edit the final manuscript, and supervised the entire project.

ACKNOWLEDGMENT

This work was supported by the Intramural Research Program of the NIH, NCI, Center for Cancer Research (grant no. ZIA BC011513).

DISCLOSURE

The authors have no conflict of interest.

ETHICS STATEMENT

Animal studies: All in vivo procedures were carried out in compliance with the Guide for the Care and Use of Laboratory Animal Resources (1996), US National Research Council, and approved by the local Animal Care and Use Committee (MIP-003; project number P214396).

ORCID

Aki Furusawa https://orcid.org/0000-0002-1339-4219
Ryuhei Okada https://orcid.org/0000-0003-3589-5054
Hiroaki Wakiyama https://orcid.org/0000-0001-6388-9888
Eisaku Kondo https://orcid.org/0000-0002-2939-036X
Hisataka Kobayashi https://orcid.org/0000-0003-1019-4112

REFERENCES

1. Sung H, Ferlay J, Siegel RL, et al. Global cancer statistics 2020: GLOBOCAN estimates of incidence and mortality worldwide for 36 cancers in 185 countries. *CA Cancer J Clin*. 2021;71:209-249.
2. Newman LA, Reis-Filho JS, Morrow M, Carey LA, King TA. The 2014 Society of Surgical Oncology Susan G. Komen for the Cure symposium: triple-negative breast cancer. *Ann Surg Oncol*. 2015;22:874-882.
3. Wu QT, Siddharth S, Sharma D. Triple negative breast cancer: a mountain yet to be scaled despite the triumphs. *Cancers*. 2021;13:3697.
4. Carey LA, Rugo HS, Marcom PK, et al. TBCRC 001: randomized phase II study of cetuximab in combination with carboplatin in stage IV triple-negative breast cancer. *J Clin Oncol*. 2012;30:2615-2623.
5. Cristofanilli M, Morandi P, Krishnamurthy S, et al. Imatinib mesylate (Gleevec) in advanced breast cancer-expressing C-kit or PDGFR-beta: clinical activity and biological correlations. *Ann Oncol*. 2008;19:1713-1719.
6. Mitsunaga M, Ogawa M, Kosaka N, Rosenblum LT, Choyke PL, Kobayashi H. Cancer cell-selective in vivo near infrared photoimmunotherapy targeting specific membrane molecules. *Nat Med*. 2011;17:1685-1691.
7. Kobayashi H, Choyke PL. Near-infrared photoimmunotherapy of cancer. *Acc Chem Res*. 2019;52:2332-2339.
8. Sato K, Ando K, Okuyama S, et al. Photoinduced ligand release from a silicon phthalocyanine dye conjugated with monoclonal antibodies: a mechanism of cancer cell cytotoxicity after near-infrared photoimmunotherapy. *ACS Cent Sci*. 2018;4:1559-1569.
9. Ogata F, Nagaya T, Okuyama S, et al. Dynamic changes in the cell membrane on three dimensional low coherent quantitative phase microscopy (3D LC-QPM) after treatment with the near infrared photoimmunotherapy. *Oncotarget*. 2017;8:104295-104302.
10. Okada R, Kato T, Furusawa A, et al. Selection of antibody and light exposure regimens alters therapeutic effects of EGFR-targeted near-infrared photoimmunotherapy. *Cancer Immunol Immunother*. 2022.
11. Okada R, Furusawa A, Vermeer DW, et al. Near-infrared photoimmunotherapy targeting human-EGFR in a mouse tumor model simulating current and future clinical trials. *EBioMedicine*. 2021;67:103345.
12. Okada R, Furusawa A, Inagaki F, et al. Endoscopic near-infrared photoimmunotherapy in an orthotopic head and neck cancer model. *Cancer Sci*. 2021;112:3041-3049.
13. Nagaya T, Okuyama S, Ogata F, Maruoka Y, Choyke PL, Kobayashi H. Near infrared photoimmunotherapy using a fiber optic diffuser for treating peritoneal gastric cancer dissemination. *Gastric Cancer*. 2019;22:463-472.
14. Sato K, Nagaya T, Choyke PL, Kobayashi H. Near infrared photoimmunotherapy in the treatment of pleural disseminated NSCLC: preclinical experience. *Theranostics*. 2015;5:698-709.
15. Nagaya T, Nakamura Y, Okuyama S, et al. Near-infrared photoimmunotherapy targeting prostate cancer with prostate-specific membrane antigen (PSMA) antibody. *Mol Cancer Res*. 2017;15:1153-1162.
16. Hayes SH, Seigel GM. Immunoreactivity of ICAM-1 in human tumors, metastases and normal tissues. *Int J Clin Exp Pathol*. 2009;2:553-560.
17. Bui TM, Wiesolek HL, Sumagin R. ICAM-1: a master regulator of cellular responses in inflammation, injury resolution, and tumorigenesis. *J Leukoc Biol*. 2020;108:787-799.
18. Tempia-Caliera AA, Horvath LZ, Zimmermann A, et al. Adhesion molecules in human pancreatic cancer. *J Surg Oncol*. 2002;79:93-100.
19. Lin YC, Shun CT, Wu MS, Chen CC. A novel anticancer effect of thalidomide: inhibition of intercellular adhesion molecule-1-mediated cell invasion and metastasis through suppression of nuclear factor-kappaB. *Clin Cancer Res*. 2006;12:7165-7173.
20. Guo P, Huang J, Wang L, et al. ICAM-1 as a molecular target for triple negative breast cancer. *Proc Natl Acad Sci U S A*. 2014;111:14710-14715.
21. Wei H, Wang Z, Kuang Y, et al. Intercellular adhesion molecule-1 as target for CAR-T-cell therapy of triple-negative breast cancer. *Front Immunol*. 2020;11:573823.
22. Guo P, Yang J, Liu D, et al. Dual complementary liposomes inhibit triple-negative breast tumor progression and metastasis. *Sci Adv*. 2019;5:eaav5010.
23. Kato T, Okada R, Furusawa A, et al. Simultaneously combined cancer cell- and CTLA4-targeted NIR-PIT causes a synergistic treatment effect in syngeneic mouse models. *Mol Cancer Ther*. 2021;20:2262-2273.
24. Maruoka Y, Furusawa A, Okada R, et al. Interleukin-15 after near-infrared photoimmunotherapy (NIR-PIT) enhances T cell response against syngeneic mouse tumors. *Cancers (Basel)*. 2020;12:2575.
25. Furusawa A, Okada R, Inagaki F, et al. CD29 targeted near-infrared photoimmunotherapy (NIR-PIT) in the treatment of a pigmented melanoma model. *Onco Targets Ther*. 2022;11:2019922.
26. Ueki Y, Saito K, Iioka H, et al. PLOD2 is essential to functional activation of integrin beta1 for invasion/metastasis in head and neck squamous cell carcinomas. *iScience*. 2020;23:100850.
27. Nagaya T, Friedman J, Maruoka Y, et al. Host immunity following near-infrared photoimmunotherapy is enhanced with PD-1 checkpoint blockade to eradicate established antigenic tumors. *Cancer Immunol Res*. 2019;7:401-413.
28. Wakiyama H, Furusawa A, Okada R, et al. Increased immunogenicity of a minimally immunogenic tumor after cancer-targeting near infrared photoimmunotherapy. *Cancers (Basel)*. 2020;12:3747.
29. Klausz K, Cieker M, Kellner C, et al. Fc-engineering significantly improves the recruitment of immune effector cells by anti-ICAM-1 antibody MSH-TP15 for myeloma therapy. *Haematologica*. 2021;106:1857-1866.
30. Hansson M, Gimsing P, Badros A, et al. A phase I dose-escalation study of antibody BI-505 in relapsed/refractory multiple myeloma. *Clin Cancer Res*. 2015;21:2730-2736.
31. Taftaf R, Liu X, Singh S, et al. ICAM1 initiates CTC cluster formation and trans-endothelial migration in lung metastasis of breast cancer. *Nat Commun*. 2021;12:4867.
32. Schroder C, Witzel I, Muller V, et al. Prognostic value of intercellular adhesion molecule (ICAM)-1 expression in breast cancer. *J Cancer Res Clin Oncol*. 2011;137:1193-1201.

33. Gkogkou P, Peponi E, Ntaskagiannis D, et al. ICAM-1 expression in patients with advanced non-small cell lung cancer treated with radiotherapy. *J BUON*. 2020;25:1779-1783.
34. Jung WC, Jang YJ, Kim JH, et al. Expression of intercellular adhesion molecule-1 and e-selectin in gastric cancer and their clinical significance. *J Gastric Cancer*. 2012;12:140-148.
35. Maeda K, Kang SM, Sawada T, et al. Expression of intercellular adhesion molecule-1 and prognosis in colorectal cancer. *Oncol Rep*. 2002;9:511-514.
36. Nagaya T, Sato K, Harada T, Nakamura Y, Choyke PL, Kobayashi H. Near infrared photoimmunotherapy targeting EGFR positive triple negative breast cancer: optimizing the conjugate-light regimen. *PLoS One*. 2015;10:e0136829.

SUPPORTING INFORMATION

Additional supporting information can be found online in the Supporting Information section at the end of this article.

How to cite this article: Fukushima H, Kato T, Furusawa A, et al. Intercellular adhesion molecule-1-targeted near-infrared photoimmunotherapy of triple-negative breast cancer. *Cancer Sci*. 2022;113:3180-3192. doi: 10.1111/cas.15466